International e-Conference on Recent Trends in Nano-Materials and Its Applications-2021
In Association with International Journal of Scientific Research in Science and Technology
Volume 9 | Issue 2 | Print ISSN: 2395-6011 | Online ISSN: 2395-602X (www.ijsrst.com)

FTIR and VSM Study of Sol-Gel Synthesized Nanoparticles Of $Mg_{0.8}Zn_{0.2}Cr_xFe_{2-x}O_4$

Swati Patil[1]*, P. M. Kharade[2], J. V. Thombare[3], R.S.Gaikwad[3], Sagar Mane[4], S. S. Dhasade[3]

[1]Department of Physics, Pratapsingh Mohite Mahavidyalaya, Karmala, Dist-Solapur, Maharashtra, India

[2]Department of Physics, Shankarrao Mohite Patil Mahavidyalaya, Akluj, Dist-Solapur, Maharashtra, India

[3]Department of Physics, Vidnyan Mahavidyalaya, Sangola, Dist-Solapur, Maharashtra, India

[4]Department of Physics, Yeungnam University, Gyeongsan, Gyeongbuk 38541, Republic of Korea

ABSTRACT

In this study, spinel magnesium zinc ferrite ($Mg_{0.8}Zn_{0.2}Cr_xFe_{2-x}O_4$: x = 0.0, 0.2, 0.4, 0.6, 0.8 and 1.0) nanoparticles were synthesized by sol-gel auto combustion method. The effects of chromium ions on the functional group and magnetic properties of spinel Mg-Zn ferrites nanocomposites were investigated. Characterization methods such as Fourier transform infrared (FT-IR) spectroscopy and vibrating sample magnetometer (VSM) were used to study functional group determination and magnetic properties of ferrite materials. With the help of FTIR, the nanoregime effect on parameters such as vibration frequency, bond length, and force constant is estimated. Using the Vibrating Sample Magnetometer (VSM), the M–H loop of $Mg_{0.8}Zn_{0.2}Cr_xFe_{2-x}O_4$ has been traced and saturation magnetization (M_s), coercivity (H_C), and retentivity (M_R) studied.

Keywords: Mg-Zn ferrites; sol-gel synthesis; FTIR; VSM.

I. INTRODUCTION

Doping of Sm and Co in bismuth ferrite will influence the properties like magnetic, structural, dielectric, ferroelectric, and leakage current density [1]. Spinel structure formation and cation distribution of ferrite powder are confirmed by using Fourier transform infrared spectroscopy with the proposed data using XRD [2]. The ability of nanoporous ferrite to dissociate water molecules has been exploited to develop a green electrical energy cell, which is a combination of electrode chemistry and material science [3]. Lithium-nickel ferrite nanocrystalline particles were synthesized by a low-temperature citrate gel auto combustion method and its structural parameters like lattice parameter, X-ray density, bulk density, and porosity has determined [4] Magnetization Mg-doped lithium ferrite decreases with increases in doping percentage of magnesium and it vanishes above the comparatively high Curie temperature Tc of 900 K [5]. By using the laser diffraction technique the dispersity of the synthesized lithium ferrite powder was investigated, it is seen that there are slight decreases in the average particle size of the ferrite powder by an increase in the mechanical milling time [6]. Copper-doped cobalt ferrite

nanoparticles show a decrease in crystallite size with an increase in doping materials, while VSM results showed that the final materials are ferromagnetic and there is a decrease in magnetization due to the decrease in the value of magnetic moments of octahedral sites[7]. Cobalt doped spinel $MgFe_2O_4$ ferrite nanocomposites with improved magneto-optical and photocatalytic properties of transition metal are seen, as cobalt content increases bandgap of ferrite material goes on increases [8]. Dye-sensitized solar cell based on FeO nanorods shows conversion efficiency of 0.43%, under the light radiation of 1000 W/m^2, which is enhanced than FeO nanoparticles [9] By increasing heating rate, the average crystallite size of sintered ferrite samples decreases, during the heating period the specific surface of nanosized Mn-Zn ferrite powder strongly enhances while the density of ferrite decrease [10] The coordinates of atoms, the dimensions of the unit cell, the occupation factors of the atom, isotropic temperature factors, as well as the interatomic distances of copper doped Mg-Zn ferrite have been determined.[11] The dielectric constant of prepared spinel ferrites decreases gradually as the concentration of rare-earth ions increases in the ferrites, this is due to the exchange of electrons between Fe^{2+} and Fe^{3+} [12] By controlling the size and composition, contrast agents of Iron oxide has been developed as T_1 or T_2 for magnetic resonance imaging (MRI), they show significant interactional T_1 and T_2 contrast effects [13] Multi ferroic samples of bismuth ferrite shows the change of rhombohedral structure to a tetragonal structure after doping of Sm and CO, further it shows an increase in the symmetry and decrease in phases, Furthermore, the dielectric properties bismuth ferrites enhance with co-doping.[14] To fabricate a magnetite-based Hydroelectric Cell a chemical method is used to synthesis mesoporous magnetite nanoparticles and its ionic diffusion of dissociated ions has been confirmed, furthermore, it is observed that due to less Ohmic loss in magnetite cell current increases [15] Mn-Zn ferrite was synthesized by simple one-pot microwave combustion method, it was observed that the magnetization values of Mn-Zn ferrites increased with increasing Mn^{2+} cation, this increased values of magnetization is due to the replacement of Zn^{2+} by Mn^{2+} in the $ZnFe_2O_4$ lattice and also due to the distribution of cations at tetrahedral and octahedral sites [16] By solution combustion method single phase Cobalt copper ferrite nanopowders with increased particle size were synthesized, with an increase of Cu^{2+} ions concentration in cobalt ferrite X-ray density increase due to increase in electron density [17]

II. EXPERIMENTAL

Nanocrystalline powders of Mg 0.8Zn0.2 Crx Fe2-x O4 were prepared by the sol-gel auto-combustion method. The A.R. grade citric acid (C6H8O7·H2O), Magnesium nitrate Mg(NO3)2.6H2O, Zinc nitrate $Zn(NO_3)_2$.6H2O, chromium nitrate (Cr(NO3)3·9H2O) and ferric nitrate Fe(NO3)3·9H2O were used as preparatory materials. Synthesis was carried out in the air atmosphere without protecting by any inert gases. The molar ratio of metal nitrates to citric acid was taken as 1:3. The metal nitrates were dissolved together in a minimum amount of double distilled water to get a clear solution. An aqueous solution of citric acid was mixed with metal nitrates solution, then ammonia solution was slowly added to adjust the pH at 7. The mixed solution was kept on a hot plate with continuous stirring at 90 °C. During evaporation, the solution became viscous and finally formed a very viscous brown gel. When finally all water molecules were removed from the mixture, the viscous gel began frothing. After few minutes, the gel automatically ignited and burnt with glowing flints. The decomposition reaction would not stop before the entire citrate complex was consumed. The auto-combustion was completed within a minute, yielding the brown-colored ashes termed as a precursor. Prepared powder was then annealed at 600 ^{0}C for 6h. finally, a fine powder with brown color was obtained.

III. RESULTS AND DISCUSSION

FTIR spectroscopy:

Fig. 1 shows the FTIR spectrum of as-synthesized powder of $Mg_{0.8}Zn_{0.2}Cr_xFe_{2-x}O_4$ in the frequency range of 800–400. The positions of the ions in the crystal through the vibrational modes of a crystal can be studied with the help of an infrared absorption spectrum. It is known that the normal cubic spinels have two IR bands representing the fundamental absorption bands.

From **Fig. 1** and **Table 1** it is observed that there are two main frequency bands, namely, the high frequency band(υ_1) is observed at 529-549 cm^{-1} whereas the lower frequency band (υ_2) is observed at 422–466 cm^{-1}. The intensity of the high frequency band(υ_1) and frequency band(υ_2) appears to increase with the addition of Cr^{3+} ions. These two observed frequency bands υ_1 and υ_2 are the characteristics of all the ferrite composites and they correspond to the intrinsic vibrations of tetrahedral and octahedral $Fe^{3+}-O_2^{2-}$ complexes, respectively. It explains that the normal mode of vibration of the octahedral cluster is lower than that of the tetrahedral cluster. From FTIR data it is seen that the normal mode of vibration of the tetrahedral cluster (529 cm^{-1}) is higher than that of the octahedral cluster (422 cm^{-1}). This can be due to the long bond length of an octahedral cluster than the tetrahedral cluster[18]. This presence of a long shoulder for the A-site is indicative of the presence of other ionic states in that site. By increasing the Cr^{3+} content in ferrite powder, the vibrational frequencies $\upsilon 1$ and $\upsilon 2$ of all the compositions change. Due to the changes in bond lengths $Fe^{3+}-O_2^{2-}$ within octahedral and tetrahedral sites, the difference in frequencies between $\upsilon 1$and $\upsilon 2$ is observed. The metal-oxygen vibrational energies increases due to the decrease in the $Fe_B^{3+}-O_2^{2-}$ intermolecular distance, which arises from the increase of the number of $Cr^{3+}-O_2^{2-}$ complexes caused by the decrease in the number of $Fe^{3+}-O_2^{2-}$ complexes and the formation of Mg^{2+}/Zn^{2+} [19].

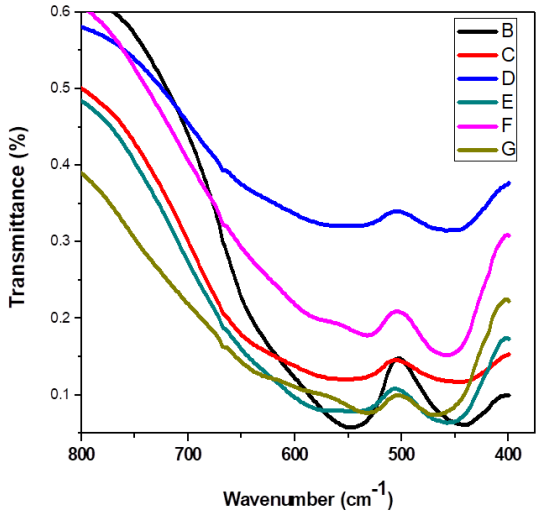

Fig.1 The FTIR spectrum of as-synthesized powder of $Mg_{0.8}Zn_{0.2}Cr_xFe_{2-x}O_4$

Comp. x	υ_1 (cm^{-1})	υ_2 (cm^{-1})	K_O x 10^4 (dyne/cm)	K_t x 10^4 (dyne/cm)
0.0	529	422	9.7603	8.5091
0.2	532	443	10.8399	8.6814
0.4	539	457	11.2090	8.6919
0.6	540	458	11.4719	8.7496
0.8	546	465	11.7285	8.8317
1.0	549	466	11.7445	8.8848

Table.1 Band position ($\nu_1$and ν_2), force constant (K_O and K_t) of $Mg_{0.8}Zn_{0.2}Cr_xFe_{2-x}O_4$.

The increasing force constant and shortening of metal-oxygen bonds of the octahedral unit is attributed to the increase in vibrational frequency (υ_2) with an increase in Cr^{3+} content in ferrite material. The force constant is the second derivative of the potential energy concerning the site radius with the other independent parameters kept constant. The force constant for the octahedral site(K_O) and tetrahedral site(K_t) were calculated by employing the Waldron method [20]. According to Waldron the

force constant K_t and K_O for respective sites are given by

$$K_t = 7.62 M_1 \nu_1^2 x10^{-3} \text{ dynes/cm} \text{----------(1)}$$

$$K_o = 10.62 \frac{M_2}{2} \nu_1^2 x10^{-3} \text{ dynes/cm} \text{----------(2)}$$

where M1 and M2 are the molecular weight of cations on the A and B sites respectively.

IV. MAGNETIC STUDIES

Substitution of Cr^{3+} ions into magnesium ferrite significantly affects the magnetic properties of ferrite materials. **Fig. 2** shows the plots of hysteresis loops for $Mg_{0.8}Zn_{0.2}Cr_xFe_{2-x}O_4$ samples. This **Fig.2** indicates that the magnesium ferrite is a soft magnetic material, which revealed minimal hysteresis. The shape and the width of the hysteresis loop depend on factors such as the porosity, grain size, and chemical composition of the compound, etc. From the field dependence of magnetization, ferrimagnetic behavior for all the samples has been observed.

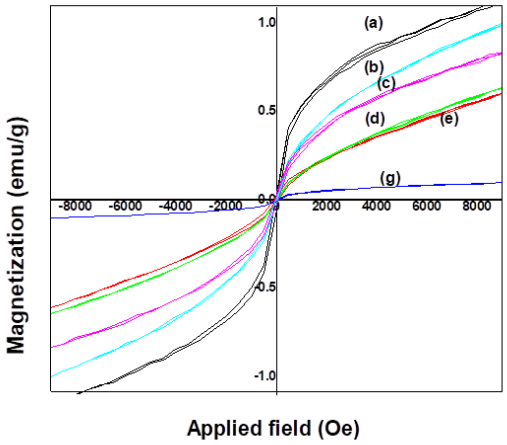

Fig. 2 Variation of magnetization with applied field measured at 300K,(a) x= 0.0, (b) x=0.2, (c) x= 0.4, (d) x=0.6, (e) x= 0.8 and(f) x= 1.0 of $Mg_{0.8}Zn_{0.2}Cr_xFe_{2-x}O_4$

From these magnetization curves (**Fig. 2)** the observed magnetic moment per formula unit,($M_{obs.}$) was determined, by extrapolating the high-field part of the curves to zero fields. In a spinel ferrite, each ion at the A site has 12 B-site ions as nearest neighbors. According to Neel's molecular field model [21], the A–B superexchange interactions dominate the intra sublattice A–A and B–B interactions. The difference of the magnetic moments of the A and B sublattices gives the net magnetic moment.[20,22]

The coercivity field, H_C reflects the coercivity for a ferromagnetic or ferrimagnetic material. This value of coercivity refers to the strength of the magnetic field required to reduce the magnetization of the ferrite magnetic sample to zero after the magnetization of the ferrite sample has reached saturation. The coercivity was observed to be significantly affected by Cr^{3+} substitution in the magnesium ferrite. It can be seen from **Fig. 3** and **Table. 2** that the coercivity increases with increasing Cr^{3+} content. According to the one-ion model, the anisotropy field in the ferrites depends on the amount of sum of effects of the different magnetic ions [23]. Values of saturation magnetization(Ms) and coercivity determined from hysteresis loops are presented in **Table 2.**

Comp. x	Ms (emu/g)	Hc (Oe)
0.0	1.1454	16.24
0.2	1.001	41.46
0.4	0.833	44.88
0.6	0.6415	56.95
0.8	0.608	61.57
1.0	0.1003	88.34

Table.2 Shows the values of magnetization(Ms), coercivity (Hc), of $Mg_{0.8}Zn_{0.2}Cr_xFe_{2-x}O_4$ with composition

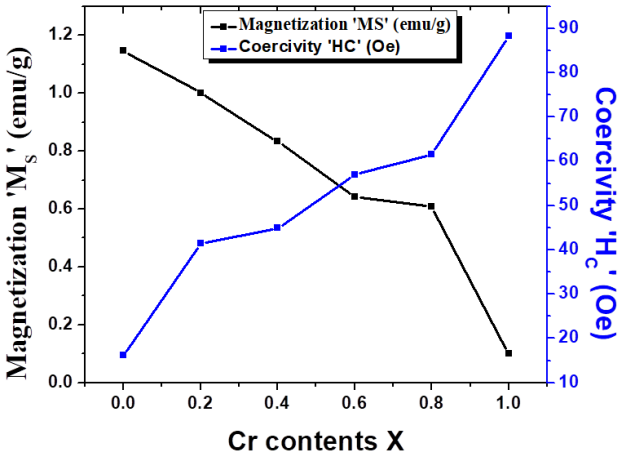

Fig. 3. Variation of saturation magnetization(M_s) and coercivity (H_C) with Cr content x.

V. CONCLUSION

The Infra-Red analysis supports the currently accepted cation distribution. With the increasing Cr^{3+} (x) content in ferrite materials, the saturation magnetization decreases linearly. The decrease in saturation magnetization is attributed to the fact that the increasing concentration of nonmagnetic Cr^{3+} ions. These nonmagnetic Cr^{3+} ions replace magnetic Fe^{3+} ions results in decreasing the value of saturation magnetization of the Mg–Zn ferrite.

VI. REFERENCES

[1]. Modified ferroelectric/magnetic and leakage current density properties of Co and Sm co-doped bismuth ferrites, Balesh Kumar Vashisth, Jarnail S. Bangruwa, Anu Beniwal, S.P. Gairola, Ashok Kumar, Nidhi Singh, Vivek VermaJournal of Alloys and Compounds, 698 (2017) 699-705

[2]. Sol-gel route of synthesis of nanoparticles of Mg Fe2O4 and XRD, FTIR and VSM study, A. Pradeep, P. Priyadharsini, G. Chandrasekaran, Journal of Magnetism and Magnetic Materials 320 (2008) 2774– 2779

[3]. Green hydroelectrical energy source based on water dissociation by nanoporous ferrite Ravinder Kumar Kotnala, and Jyoti Shah, Int. J. Energy Res. 40 (2016) 1652-1661

[4]. Structural and Electrical Properties of Li–Ni Nanoferrites Synthesised by Citrate Gel Autocombustion Method, G. Aravind, D. Ravinder, and V. Nathanial, Physics Research International, Volume 2014, Article ID 672739, 11 pages

[5]. Magnetic study of nanocrystalline Mg-doped lithium ferrite, Marek Pekala, Frank J. Berry, Hisham M Widatallah, Czechoslovak Journal of Physics, 52 (2002) 101-104

[6]. Influence of mechanical milling conditions on the dispersity of lithium ferrite, S A Lamonova, E N Lysenko and A V Malyshev, Materials Science and Engineering 93 (2015) 012035

[7]. Structural characterization and magnetic properties of undoped and copper-doped cobalt ferrite nanoparticles prepared by the octanoate coprecipitation route at very low dopant concentrations, Hypolite Mathias Kamta Tedjieukeng, Patrice Kenfack Tsobnang, Roussin Lontio Fomekong, Ekane Peter Etape, Pattayil A. Joy, Arnaud Delcortee and John Ngolui Lambia, Royal Society of Chemistry, 8 (2018) 38621–38630

[8]. Enhanced magneto-optical and photocatalytic properties of transition metal cobalt (Co2+ ions) doped spinel MgFe2O4 ferrite nanocomposites, A. Godlyn Abraham, A. Manikandan, E. Manikandan, S. Vadivel, S.K. Jaganathan, A. Baykal, P. Sri Renganathan, Journal of Magnetism and Magnetic Materials, 452 (2018) 380-388

[9]. One-Pot Low Temperature Synthesis and Characterization Studies of Nanocrystalline α-Fe2O3 Based Dye Sensitized Solar Cells, A. Manikandan, A. Saravanan, S. Arul Antony, and M. Bououdina, Journal of Nanoscience and Nanotechnology, 15 (2015) 4358–4366

[10]. Sintering of Nanosized Mn-Zn Ferrite Powders, Marko Rozman and Miha Drofenik, American Ceramic Society, 81(1998) 1757–64
[11]. Application of Rietveld Method to the Structural Characteristics of Substituted Copper Ferrite Compounds, S. Ahmed Farag, M. A. Ahmed, S. M. Hammad, A. M. Moustafa, Cryst. Res. Technol., 36 (2001) 85–92
[12]. Structural and dielectric properties of copper-based spinel ferrites, The European Physical Journal Plus, Hafiz Muhammad Tahir Farid,Ishtiaq Ahmad, Irshad Ali, Asif Mahmood, and Shahid M. Ramay, 41 (2018) 133
[13]. Interplay between Longitudinal and Transverse Contrasts in Fe3O4 Nanoplates with (111) Exposed Surfaces, Zijian Zhou,Zhenghuan Zhao,Hui Zhang,Zhenyu Wang, Xiaoyuan Chen, Ruifang Wang,Zhong Chen, and Jinhao Gao, ACS anao, 8 (2014) 7976–7985
[14]. Modified ferroelectric/magnetic and leakage current density properties of Co and Sm co-doped bismuth ferrites, Balesh Kumar Vashisth1, Jarnail S. Bangruwa, Anu Beniwal, S.P. Gairola, Ashok Kumar, Nidhi Singh, Vivek Verma, Modified ferroelectric/magnetic and leakage current density properties of Co and Sm co-doped bismuth ferrites, Journal of Alloys and Compounds, 698, (2017) 699-705
[15]. Environment-Friendly Mesoporous Magnetite Nanoparticles-Based Hydroelectric Cell Shipra Jain, Jyoti Shah, S. R. Dhakate, Govind Gupta, C. Sharma, and R. K. Kotnala, J. Phys. Chem. C, 122 (2018) 5908–5916
[16]. Enhanced Catalytic Activity and Magnetic Properties of Spinel MnxZn1–xFe2O4 ($0.0 \leq x \leq 1.0$) Nano-Photocatalysts by Microwave Irradiation Route,G. Padmapriya, A. Manikandan, V. Krishnasamy, Saravana Kumar Jaganathan, S. Arul Antony, Journal of Superconductivity and Novel Magnetism, 29(2016) 8-16
[17]. Role of Cu2+ ions substitution in magnetic and conductivity behaviour of nano CoFe2O4, D.M. Jnaneshwara, D.N. Avadhani, B. Daruka Prasad, H. Nagabhushana,B. M. Nagabhushana, S.C. Sharma, S. C. Prashantha, C. Shivakumaraha, Spectrochimica Acta Part A: Molecular and Biomolecular Spectroscopy, 132 (2014) 256-262
[18]. R.D.Waldron,Phy.Rev.99(1955)1727
[19]. O.Hemeda,M.A.Amer,S.AboulEnein,M.A.Ahmed,Phys.StatusSolidiA156 (1996) 29.
[20]. R.D.Waldron,Phy.Rev.99(1955)1727
[21]. L. Neel, Ann. Phys. 3 (1948) 137
[22]. L. Neel, C.R.Acad.,Sci.Paris230(1950)375
[23]. S.Chikazumi, S.Charap, Physics of Magnetism, John Wiley & Sons, NewYork,1964. (pp.153).